A: Environmental, Combustion, and Atmospheric Chemistry; Aerosol Processes, Geochemistry, and Astrochemistry

Unimolecular Reactions of Peroxy Radicals Formed in the Oxidation of #-pinene and #-pinene by Hydroxyl Radicals

Lu Xu, Kristian H. Møller, John D. Crounse, Rasmus V. Otkjær, Henrik Grum Kjaergaard, and Paul O. Wennberg

J. Phys. Chem. A, **Just Accepted Manuscript** • DOI: 10.1021/acs.jpca.8b11726 • Publication Date (Web): 31 Jan 2019

Unimolecular Reactions of Peroxy Radicals Formed in the Oxidation of α-pinene and β-pinene by Hydroxyl Radicals

Lu Xu[†,*], Kristian H. Møller[§], John D. Crounse[†], Rasmus V. Otkjær[§], Henrik G. Kjaergaard[§,*], Paul O. Wennberg[†,⊥,*]

[†]Division of Geological and Planetary Sciences, California Institute of Technology, Pasadena, California 91125, United States

[§]Department of Chemistry, University of Copenhagen, Universitetsparken 5, DK-2100, Copenhagen Ø, Denmark

[⊥]Division of Engineering and Applied Science, California Institute of Technology, Pasadena, California 91125, United States

Abstract

Atmospheric oxidation of monoterpenes (emitted primarily by evergreen trees) is known to contribute to the formation and growth of aerosol particles. While recent research has tied the formation of organic aerosol to unimolecular chemistry of the organic peroxy radicals (RO_2) formed in the oxidation of monoterpenes, the fundamental physical chemistry of these RO_2 remains obscure. Here, we use isomer-specific measurements and *ab initio* calculations to determine the unimolecular reaction rates and products of RO_2 derived from the hydroxyl radical (OH) oxidation of α-pinene and β-pinene. Among all the structural isomers of the first-generation RO_2 from both monoterpenes, we find that the first-generation RO_2 produced following opening of the four-membered ring undergo fast unimolecular reactions (4±2 and 16±5 s^{-1} for α-pinene and β-pinene, respectively) at 296 K, in agreement with high level *ab initio* calculations. The presence of the hydroxy group and carbon-carbon double bond in the ring-opened RO_2 enhances the rates of these unimolecular reactions, including endo-cyclization or H-shift via transition states involving six- and seven-membered rings. These reaction rate coefficients are sufficiently fast that unimolecular chemistry is the dominant fate of these monoterpene derived RO_2 in the atmosphere. In addition, the overall yield of first generation α-pinene and β-pinene hydroxy nitrates, $C_{10}H_{17}NO_4$, at 296 K and 745 torr is measured to be 3.3±1.5% and 6.4±2.1%, respectively, for conditions where all RO_2 are expected to react with NO ([NO] > 1000 ppbv). These yields are lower than anticipated.

Introduction

Approximately 150 Tg of monoterpenes ($C_{10}H_{16}$) are emitted from biogenic vegetation to Earth's atmosphere every year[1]. Monoterpenes rapidly react with atmospheric oxidants and produce a myriad of oxygenated compounds[2-7] that influence the NO_x cycle[8] and Earth's radiation balance[9]. Oxygenated compounds produced from monoterpenes are a major contributor to organic aerosol globally[10-11] and have been suggested to be the largest source of summertime organic aerosol in the southeastern U.S.[7, 12]. Despite extensive investigations, knowledge of the mechanisms and products of monoterpene photooxidation is still incomplete[13]. In particular, the fate of peroxy radicals (RO_2) produced in this chemistry remains speculative. Typically, RO_2 in the atmosphere undergo bimolecular reactions with nitric oxide (NO), hydroperoxy radical (HO_2), and other RO_2[14-15]. Recent studies have shown, however, that RO_2 unimolecular reactions can often compete with these bimolecular reactions[16-20]. Some monoterpene RO_2 have been inferred to undergo fast unimolecular reactions, based on the observed rapid formation of highly oxygenated molecules (HOMs), which carry six or more oxygen atoms in the oxidation of monoterpenes[9, 21-22]. The unimolecular reaction rates of monoterpene RO_2, however, have not been measured.

In this study, we experimentally determine the unimolecular reaction rate coefficients of RO_2 derived from the OH oxidation of α-pinene and β-pinene, which together account for more than half of total monoterpene emissions[1]. We perform isomer-specific measurements of a suite of hydroxy nitrates (HNs), produced from RO_2 reaction with NO, to probe the competition between RO_2 bimolecular and unimolecular reactive pathways. We also use *ab initio* multi-conformer transition state theory (MC-TST) [23-24] to aid the understanding of the reaction mechanisms.

Methods

Experimental Methods. We perform a suite of laboratory photooxidation experiments of α-pinene and β-pinene in a 0.8 m^3 collapsible FEP Teflon (Dupont) Environmental Chamber at ambient laboratory pressure (~993 hPa) and temperature (296 K). The VOC ((+) α-pinene (98%, Sigma-Aldrich) or (-) β-pinene (99%, Sigma-Aldrich)) is transferred into the experimental chamber via a gas-tight 500 cm^3 glass bulb. We prepare the bulb by evacuating it to <0.3 torr, evaporating VOC liquid into the bulb, and serial dilution with N_2 to achieve the desired mixing ratio. The concentration of VOC in glass bulb is verified by FTIR spectroscopy using tabulated cross-sections [25]. The initial VOC concentration in the chamber ranges from roughly 60 to 120 ppbv.

The photolysis of methyl nitrite (CH_3ONO) is used as the primary source of OH. CH_3ONO is synthesized, purified, and stored using methods similar to those described by Taylor et al. [26] The CH_3ONO is injected into the chamber in the same fashion as VOC. The initial CH_3ONO concentration in the chamber is roughly 70 ppbv. For experiments with initial NO, a 500 cm^3 bulb with desired NO concentration is prepared by mixing 1993 ± 20 ppmv NO (Matheson) and N_2 with the desired dilution ratio. The content of the bulb is then transferred to the chamber. The initial NO concentration ranges from 0 to 2.2 ppmv. Dry zero air is added to the evacuated chamber using a mass flow controller (MKS), allowing the initial concentration of species to be calculated to better than 5% uncertainty. The detailed concentrations of VOC, NO, and CH_3ONO in all experiments are shown in Table S1. After all of the reagents are injected and well-mixed in the chamber, UV lights (Sylvania F40/350BL) are turned on to initiate photooxidation. To study the RO_2 unimolecular reactions under low concentrations of NO and HO_2, we use only one UV bulb. The OH concentration ranges from 1×10^6 to 8×10^6 molecule cm^{-3}, due to different NO levels

between experiments. To achieve similar OH exposure (i.e., 2×10^9 and 1×10^9 molecules cm^{-3} s for α-pinene and β-pinene experiments, respectively), we vary the oxidation time between 2.5 min to 30 min. Under these OH exposure levels, roughly 10% of initial VOC is oxidized.

Instrumentation. The analytical instruments, including an O_3 monitor (Teledyne O_3 M400E), a chemilumnescence NO/NO_x monitor (Teledyne NO_x M200EU), a Gas Chromatograph with a Flame Ionization Detector (GC-FID, Hewlett Packard 5890 series II Plus), and a Gas-Chromatography Time of Flight Chemical Ionization Mass Spectrometer (GC-ToF-CIMS), are connected to experimental chamber using ~2 m of 1/4 inch PFA tubing. We use the GC-FID to measure α-pinene and β-pinene. Because CH_3ONO can cause interference in the measured concentrations of NO and NO_2, the NO_x monitor is only used to measure the initial NO and NO_2 concentration (before CH_3ONO injection). The O_3 concentration measured by the O_3 monitor is close to zero in all experiments, which limits VOC consumption by O_3 to less than 1% during these experiments.

We use GC-ToF-CIMS with CF_3O^- as the reagent ion, which is sensitive to multifunctional oxygenated products. CF_3O^- is produced by flowing 1 ppmv CF_3OOCF_3 (in N_2) through a radioactive ^{210}Po source. Then, CF_3O^- selectively interacts with analytes at a pressure of 35 mbar to generally form either cluster ions (R1) or fluoride transfer ions (R2).

$$VOC + CF_3O^- \leftrightarrow VOC\bullet CF_3O^- \quad (R1)$$
$$VOC + CF_3O^- \rightarrow VOC^-_{-H}\bullet HF + CF_2O \quad (R2)$$

The GC-ToF-CIMS has two sampling modes, direct sampling and GC sampling. In direct sampling mode, CIMS samples air directly from the reaction chamber recording spectra at 10 Hz temporal resolution. In GC sampling mode, the CIMS samples the effluent of a GC. In brief, the analytes are pulled from the reaction chamber and cryo-trapped on the head of a 1 m Restek RTX-

1701 column at -20ºC. After trapping for certain time (typically 10 min, 2 L chamber air), elution is enabled using a flow of 5 sccm N_2 and a temperature ramping program (SI section S1). The GC effluent is diluted with additional N_2 and transferred into the CIMS. More details about the operation and principles of CF_3O^- GC-ToF-CIMS can be found in Vasquez et al[27]. In both sampling modes, the observed ion signals are normalized to the sum of isotopes of the reagent ion (i.e., $^{13}CF_3O^-$ and $^{13}CF_3O^-\bullet H_2O$), to account for variation in the total ion signal. The high mass resolution data analysis is performed using the Tofware software (Tofwerk).

Peroxy radical bimolecular lifetime. We perform a series of experiments under different RO_2 bimolecular lifetimes ($\tau_{bimolecular}$, Eqn.(1)) by varying [NO] and [HO_2].

$$\tau_{bimolecular} = \frac{1}{k_{RO_2+NO}[NO] + k_{RO_2+HO_2}[HO_2]} \quad \text{Eqn. (1)}$$

The [NO] and [HO_2] during photooxidation are simulated using Master Chemical Mechanism (MCM, version 3.2)[28-29] updated with nitrate branching ratios and ring-opening fractions of activated terpene alkyl radicals based on results from this study. k_{RO2+NO} and $k_{RO2+HO2}$ are taken from the MCM[29] as 9.15×10^{-12} and 2.39×10^{-11} cm^3 $molec^{-1}$ s^{-1} at 296 K, respectively. We assume k_{RO2+NO} and $k_{RO2+HO2}$ to be isomer independent. RO_2+RO_2 chemistry is calculated to be of negligible importance in these experiments due to small concentrations of RO_2 radicals. We use MCM and estimate that RO_2+RO_2 reactions account for < 2% of RO_2 bimolecular loss, using a rate coefficient of 2×10^{-12} cm^3 $molec^{-1}$ s^{-1}. Details about the MCM updates and $\tau_{bimolecular}$ calculation can be found in the SI section S2. For experiments with no initial NO injection (i.e., Experiments 6 and 13 in Table S1), we estimate [NO] and [HO_2] based on the measured production rates of H_2O_2, hydroxy hydroperoxides, and hydroxy nitrates by following the procedure in

Crounse et al.[30] The subsequently calculated $\tau_{bimolecular}$ from this method agree within 25% of the values estimated using MCM (SI section S2).

Computational approach. Reaction rate coefficients, *k*, for the RO_2 unimolecular reactions are calculated using MC-TST[23-24]:

$$k = \kappa \frac{k_B T}{h} \frac{\sum_i^{All\ TS\ conf.} \exp\left(-\frac{\Delta E_i}{k_B T}\right) Q_{TS_i}}{\sum_j^{All\ R\ conf.} \exp\left(-\frac{\Delta E_j}{k_B T}\right) Q_{R_j}} \exp\left(-\frac{E_{TS} - E_R}{k_B T}\right) \quad \text{Eqn. (2)}$$

where κ is the tunneling coefficient, k_B is the Boltzmann constant, T is the temperature and h is the Planck constant. The two summations run over all transition states and reactant conformers, respectively, and sum the partition function of a given conformer weighted by its Boltzmann factor calculated relative to the corresponding lowest-energy conformer. The final exponential term has the zero-point corrected energy difference between the lowest-energy TS and reactant conformers, i.e., the reaction barrier.

Energies and partition functions in the equation are calculated using the approach described by Møller *et al.*[23] Briefly, conformers are located by a systematic conformer search using MMFF in Spartan '14 or '16 with a neutral charge enforced [31-38]. The conformer search is followed by optimizations with B3LYP/6-31+G(d) in Gaussian 16, rev. A.03 [39-44]. Slow reactions (i.e. with rate coefficients below 5×10^{-3} s^{-1} at room temperature) are ignored, because the calculated rate coefficients at this level of theory are most often biased high. For the faster reactions, conformers with electronic energies within 2 kcal mol^{-1} of the lowest-energy conformer at the B3LYP/6-31+G(d) level are reoptimized using ωB97X-D/aug-cc-pVTZ [45-47]. In Møller et al., a 2 kcal mol^{-1} cut-off based on electronic energy at this level was found to be suitable [23]. For the conformer lowest in zero-point corrected energy at the ωB97X-D/aug-cc-pVTZ level, an RO-CCSD(T)-F12a/VDZ-F12//ωB97X-D/aug-cc-pVTZ (abbreviated F12) single-point energy calculation is

done to get a more accurate barrier height [48-54]. Due to issues with the HF calculations converging to different possible solutions, no F12 single-point energy calculations are conducted for abstraction from OH groups. Consistent with Møller et al.[55], we estimate that the uncertainty on the rate coefficients increases to a factor of 100 without F12 single point energy calculations.

The tunneling coefficient is calculated using the Eckart approach based on the conformers connected to the lowest-energy TS using an IRC[56-57]. Eckart barriers are calculated using F12, while the imaginary frequency of the TS is calculated at the ωB97X-D/aug-cc-pVTZ level. The conformer searches are performed using Spartan '14 or '16, the DFT calculations are done with Gaussian 16, rev. A.03 and the F12 calculations are conducted using Molpro 2012. For reaction A1, the DFT calculations are performed using Gaussian 09, rev. D.01.

The competition between ring-opening and addition of O_2 for the hydroxy alkyl radicals formed by addition of OH to α-pinene and β-pinene is modeled using RRKM theory within the MESMER software package[58] with electronic structure theory as described in the approach of Møller et al.[23] A full description of the theoretical approach is included in SI section S3. The dipole moment and polarizability of oxidation products, for use in estimating instrumental sensitivity, are calculated using B3LYP/cc-pVTZ (SI section S3).

Following the recommendations of previous studies and comparisons with experiments, we estimate the uncertainty on rate coefficients of this approach to be a factor of 10 [18, 23, 59]. Our calculated results are broadly consistent with previous studies by Vereecken et al.[5, 60], Peeters et al.[61], and Berndt et al.[21], but use higher level of theory and include important pathways not previously considered.

Results and Discussion

The isomer distribution of $C_{10}H_{17}NO_4$ hydroxy nitrates. The oxidation of both monoterpenes initiated by OH addition produces a set of RO_2 isomers and, following reaction with NO, hydroxy nitrates (HNs). Here, we only describe the formation of $C_{10}H_{17}NO_4$. As discussed later, additional nitrates are formed following isomerization chemistry of peroxy and alkoxy radicals. A simplified oxidation mechanism for α-pinene + OH is shown in Scheme 1. The OH addition onto the double bond produces four hydroxy alkyl radicals, two diastereomer pairs of 2-OH,3-R• and 3-OH,2-R•. It is expected that 2-OH,3-R• mainly undergoes collisional stabilization, followed by O_2 addition to produce 2-OH,3-RO_2. 3-OH,2-R•, however, can undergo either collisional stabilization and O_2 addition to produce 3-OH,2-RO_2 or, via C-C scission (ring opening) and O_2 addition, form 3-OH,8-RO_2[4]. In total, three distinct structural isomers of RO_2 (each comprised of several stereoisomers) are produced. As a result, three structural isomers of HNs are formed via RO_2 reaction with NO. A similar scheme for β-pinene is shown in Scheme S1.

The HNs are separated using gas chromatography and quantified by GC-ToF-CIMS (Figure 1). Three distinct peaks are observed to be produced from the OH oxidation of both monoterpenes in the presence of NO. The structural assignment of the HN isomers is achieved through several experiments. The ring-opened HN is unsaturated and thus reacts with O_3 while the ring-retained HN isomers are saturated and will not do so (Figure S1). Thus, the third peak is assigned to ring-opened HN (i.e., 3-OH,8-ONO_2 for α-pinene) because it disappears upon adding O_3 to the chamber following photooxidation. The first peak in the chromatogram is assigned to the HN with the –ONO_2 group on the less-substituted carbon (i.e., 2-OH,3-ONO_2 for α-pinene). This assignment is based on the elution time of the major HN produced from NO_3-initiated oxidation experiments (Figure S2), where the first peak corresponds to the dominant peak produced from

NO_3 chemistry, consistent with the assumption that NO_3 reacts with alkenes by primarily adding to the less-substituted olefinic carbon[62]. Finally, the second peak is assigned to the HN with the –OH group on the less-substituted carbon (i.e., 3-OH,2-ONO_2 for α-pinene). This assignment is based on the previous finding that the retention order for HNs with similar structures generally follows the order: tertiary –OH, secondary –OH, and then primary –OH for the same GC column[63] (Figure S3). This observation has a plausible rationale as the secondary –OH has stronger interaction with GC column than tertiary OH due to less shielding effects. More details on chromatographic assignment are provided in the SI section S1. In summary, for each monoterpene, the first two peaks are the two structural isomers of ring-retained β-HNs (e.g., 2-OH,3-ONO_2 and 3-OH,2-ONO_2 for α-pinene), each likely comprised of multiple diastereomers; the third peak is the ring-opened HN (e.g., 3-OH,8-ONO_2 for α-pinene), likely containing 2 diastereomers for the α-pinene system.

For conditions where all RO_2 are expected to react with NO ([NO] > 1000 ppbv), the GC transmission efficiencies of α-pinene and β-pinene hydroxy nitrates ($C_{10}H_{17}NO_4$) are 79±4% and 99±5%, respectively (SI section S1).

Rate Coefficients of Unimolecular Reactions. We find that the yields of ring-retained β-HNs (i.e., the amount of HNs produced divided by the amount of monoterpene oxidized) do not change with RO_2 bimolecular lifetime ($\tau_{bimolecular}$), after accounting for the fraction of RO_2 that reacts with NO (Figure S4). This finding suggests that the unimolecular reaction rates of ring-retained RO_2 are much slower than bimolecular chemistry for conditions investigated here ($\tau_{bimolecular}$: 0.001 – 10 s). This experimental result is corroborated by our MC-TST calculations using ωB97X-D/aug-cc-pVTZ; the unimolecular reaction rate coefficients for ring-retained RO_2 in both monoterpenes are calculated to be slower than 0.05 s^{-1} with the exception of one isomer of α-pinene which has a

calculated H-shift rate coefficient of 0.12 s^{-1} (Table S8 and S9). In contrast, we find that the yield of ring-opened HN (i.e., α-pinene 3-OH,8-ONO_2 and β-pinene 1-OH,8-ONO_2) decreases with $\tau_{bimolecular}$. Figure 1(a) and (b) present the HN distributions under three different $\tau_{bimolecular}$ for the α-pinene and β-pinene systems, respectively. The yield of ring-opened HNs decreases with longer $\tau_{bimolecular}$, because the unimolecular reactions shorten the time available for the ring-opened RO_2 to react with NO. This observation is corroborated by our theoretical calculation as will be shown later.

To determine the unimolecular reaction rates of ring-opened RO_2, we utilize the ratio of the ring-opened HN signal relative to that of the ring-retained HNs. Ring-retained HNs are used as a reference for the RO_2 + NO bimolecular reaction, as the unimolecular reactions of ring-retained RO_2 are negligible for the conditions investigated here. In contrast, the formation of ring-opened HN depends on the competition between reaction with NO and unimolecular chemistry. Thus, the change in the (ring-opened HN):(ring-retained HNs) ratio as a function of $\tau_{bimolecular}$ is a measure of the ratio of the unimolecular reactions of ring-opened RO_2 to its bimolecular reaction with NO. Detailed mathematical derivations are shown in the SI section S2. The (ring-opened HN):(ring-retained HNs) ratio decreases as $\tau_{bimolecular}$ increases due to increased importance of the unimolecular reactions of the ring-opened RO_2 at longer $\tau_{bimolecular}$ (Figure 2). When $\tau_{bimolecular}$ is ~10 s, the formation of ring-opened HN is suppressed because all ring-opened RO_2 undergoes unimolecular reactions. We use a kinetic model to simulate the relationship between (ring-opened HN):(ring-retained HNs) and $\tau_{bimolecular}$ (SI section S4) with varying unimolecular reaction rates. The unimolecular reaction rate coefficient is the only fitted parameter in the model. By comparing the simulated and measured relationships, we determine the rates of unimolecular reactions to be 4±2 s^{-1} and 16±5 s^{-1} at 296 K for α-pinene and β-pinene ring-opened RO_2, respectively (Figure 2).

An equivalent NO reactivity at 296 K requires mixing ratios of 18 and 70 ppbv NO, respectively – values substantially larger than found over forested regions where monoterpenes are emitted and even over many polluted urban areas [64-65].

These rates are consistent with the previously estimated ranges from theoretical calculations (1-10 s^{-1} for α-pinene ring-opened RO_2 in Berndt et al.[21] and Vereecken et al.[60]) and from simulating α-pinene ozonolysis with a few fitting parameters (3-10 s^{-1} in Zhao et al.[22]). The measured rates agree well with our theoretical calculations using higher level of theory as presented in the next section.

Unimolecular reaction channels. For the ring-opened RO_2 from both monoterpenes, there are a suite of potential unimolecular reaction channels (Scheme 2). The channel-specific rate coefficients are calculated with the MC-TST approach from Møller et al.[23] (Table S6 and S7). α-pinene ring-opened RO_2 (i.e., 3-OH,8-RO_2) exist in both *syn* and *anti* isomers, depending on the relative positions of the –OH and the -$C(CH_3)_2OO$ groups (Scheme 2a and 2b). For the experimental configuration used in this study we are unable to separate HNs derived from the *syn* and *anti* ring-opened RO_2, and thus we experimentally infer the isomer-averaged sum of unimolecular reaction rates of the precursor RO_2's. For *anti* 3-OH,8-RO_2, the fastest unimolecular pathway is calculated to be the 1,5 H-shift from C6 (1.1 s^{-1}), followed by the 1,6 H-shift from C3 (0.37 s^{-1}) and the endo-cyclization to C7 (0.35 s^{-1}) at 298.15 K. The remaining unimolecular reactions are calculated to be very slow (< ~10^{-3} s^{-1}). The rate of 1,5 H-shift from C6 is enhanced due to stability of the nascent allylic radical. While the 1,6 H-shift from C3 also forms an allylic radical, the calculated rate is slower than the 1,5 H-shift from C6, which is likely because the 1,6 H-shift requires a greater distortion of the ring inducing more ring-strain (Figure S5). In addition to H-shift, *anti* 3-OH,8-RO_2 can undergo endo-cyclization to form bicyclic alkyl radical. The endo-

addition at C7 is favored over the endo-addition at C2, as the former yields a tertiary alkyl radical with a six-membered ring. The calculated summed rate of unimolecular reactions of all channels for *anti* 3-OH,8-RO_2 is 1.8 s^{-1} at 298.15 K. For *syn* 3-OH,8-RO_2, the dominant isomerization pathway is predicted to be endo-addition to C7 (2.3 s^{-1}), followed by 1,5 H-shift from C6 (0.16 s^{-1}). Unlike *anti* 3-OH,8-RO_2, *syn* 3-OH,8-RO_2 cannot undergo a 1,6 H-shift from C3 because the peroxy radical and C3-H are on opposite sides of the six-membered ring. The summed rate of unimolecular reactions of *syn* 3-OH,8-RO_2 is 2.5 s^{-1} at 298.15 K. Assuming that *anti* and *syn* 3-OH,8-RO_2 are initially produced in equal abundance, we find that the calculated average rate of unimolecular reactions of 3-OH,8-RO_2 (2.1 s^{-1}) agrees with the measured value (4±2 s^{-1}), within uncertainty.

In the β-pinene system, the ring-opened RO_2 (i.e., 1-OH,8-RO_2) only has one chiral center. We do not distinguish between enantiomers, as their unimolecular reaction rate coefficients are the same. We calculate that 1-OH,8-RO_2 primarily undergoes endo-cyclization to C7 (4.0 s^{-1}), 1,5 H-shift from C6 (1.4 s^{-1}), and 1,6 H-shift from C3 (0.28 s^{-1}) at 298.15 K. The summed rate of unimolecular reactions of 1-OH,8-RO_2 (5.7 s^{-1}) agrees with the measured value (i.e., 16±5 s^{-1}), within uncertainty. The calculated endo-cyclization rate coefficients of β-pinene 1-OH,8-RO_2 and α-pinene *syn* 3-OH,8-RO_2 are roughly 10 times faster than that of α-pinene *anti* 3-OH,8-RO_2. This is likely because β-pinene 1-OH,8-RO_2 and α-pinene *syn* 3-OH,8-RO_2 exhibit a hydrogen bond interaction between the –OH and –OO, stabilizing the transition state (Figure S6). This option is not available to the *anti* 3-OH,8-RO_2 as the two functional groups are on opposite sides of the ring.

Reaction Products of Ring-Opened RO_2 under long $\tau_{bimolecular}$. In experiments with long $\tau_{bimolecular}$, we detect several stable end products that appear to arise from the unimolecular reactions. For α-pinene, we observe two peaks in the chromatogram of *m/z* 332 ($C_{10}H_{17}NO_6 \cdot CF_3O^-$),

corresponding to the mass of organic nitrates P1 and P4-P6 (Scheme 3) produced from secondary generation RO_2 (R1, R4-R6) reaction with NO. To probe the identity of compounds at *m/z* 332, we add O_3 to the reaction chamber after photooxidation to test for the presence of C-C double bonds. Both peaks at *m/z* 332 in GC chromatography are still present after O_3 addition (Figure S7). In addition, tests are conducted through adding D_2O to the GC eluent to determine the number of exchangeable H atoms (-OH and –OOH groups) in the molecules by H/D exchange reactions. The H/D analysis reveals only one exchangeable H atom in $C_{10}H_{17}NO_6$. These tests suggest that the compounds detected at *m/z* 332 are saturated with one acidic H (e.g., isomers of P1) rather than unsaturated with two acidic H's (e.g., P4-P6). The lack of P4-P6 formation is likely because either their precursor RO_2 (R4-R6) undergo unimolecular reactions (as discussed below and shown in Scheme S4) or that P4-P6 have poor transmission efficiency through the GC.

A co-product of P1 from R1 reaction with NO is alkoxy radical R2. The likely fate of R2 is decomposition via two scission channels, both of which can lead to products sharing the same chemical formula, $C_{10}H_{16}O_4$ (endoperoxide ketoaldehyde P2 and hydroxy diketone aldehyde P3 in Scheme 3). At long $\tau_{bimolecular}$ (i.e., 2.4 s in Figure 3), we detect one peak in the chromatogram of *m/z* 285 ($C_{10}H_{16}O_4 \cdot CF_3O^-$). The H/D exchange analysis suggests that this peak does not have any exchangeable H, implying the presence of P2, instead of P3 (has one –OH group). This observation is consistent with our and earlier theoretical calculations[60] that the major decomposition pathway of R2 is scission towards the –OH group to produce R3 and subsequently P2 (Table S13). The assignment of P2 is further supported in that the signal from this peak is highly correlated with P1, which originates from the same precursor RO_2 (i.e., R1) (Figure S8).

One oxidation product of the 1,6 H-shift of the hydrogen attached to C3 for α-pinene *anti* 3-OH,8-RO_2 is a hydroperoxide ketone ($C_{10}H_{16}O_3$, P7 in Scheme 3), generated by O_2 addition to

C3 in the alkyl radical and subsequent HO_2 elimination. This product is assigned to one peak in the chromatogram of *m/z* 269 ($C_{10}H_{16}O_3{\cdot}CF_3O^-$) (Figure S9), because this peak has one exchangeable H, a C-C double bond, and increases with longer $\tau_{bimolecular}$ (Figure 4).

For β-pinene, the endo-cyclization channel is calculated to account for 70% of the RO_2 unimolecular reactivity based on MC-TST calculated rates. Similar to α-pinene, the endo-cyclization channel produces an endoperoxide hydroxy nitrate after reaction with O_2 and NO, the observed formation of which is enhanced under longer $\tau_{bimolecular}$ (Figure 4). The alkoxy radical from the endo-cyclization channel (similar to R2 in Scheme 3) is calculated to primarily break the carbon-carbon bond attached to the endocyclic peroxide and subsequently decompose (Scheme S6).

Reaction Products of Ring-Opened RO_2 under short $\tau_{bimolecular}$. In α-pinene experiments with short $\tau_{bimolecular}$, we also observe a number of stable end products (Scheme 4). We observe a CIMS signal at *m/z* 316 ($C_{10}H_{17}NO_5{\cdot}CF_3O^-$). A product with the same mass (MW 231 amu) has been detected and proposed to be dihydroxy nitrate by Aschmann et al. [66] However, H/D exchange analysis reveals only one acidic H in this product. One possible pathway to form the detected products at *m/z* 316 is endo-cyclization of ring-opened hydroxy alkoxy radical (calculated earlier to have an extremely low barrier [60]), followed by reaction with O_2 and NO to produce nitrate P8 as shown in Scheme 4. This proposed structure is further supported by the O_3 test, which suggests the absence of C-C double bond in the compound. At short $\tau_{bimolecular}$, we also observe a GC peak at *m/z* 285 ($C_{10}H_{16}O_4{\cdot}CF_3O^-$), which shares the same chemical formula, but different retention time as P2 produced at long $\tau_{bimolecular}$ (Figure 3). Aschmann et al. also observed a signal for a compound of molecular weight 200 amu (e.g., $C_{10}H_{16}O_4$) [66] at short $\tau_{bimolecular}$. They assigned this signal to a trihydroxy carbonyl. Our H/D exchange analysis reveals, however, that this product does not have

any acidic H. The lack of acidic H in $C_{10}H_{16}O_4$ is consistent with the dicarbonyl ketone ester proposed by Vereecken et al. [60] (P9 shown in Scheme 4). Finally, multiple isomers are resolved at *m/z* 269 ($C_{10}H_{16}O_3 \cdot CF_3O^-$, Figure S9) and all contain one exchangeable H. Previously proposed structures for compounds with this mass have more than one –OH or –OOH group [66].

Potential Routes to Form Highly Oxygenated Organic Compounds. In addition to producing the end products discussed above, the second-generation RO_2 (e.g., R4-R6 in Scheme 3) can undergo further unimolecular reactions at enhanced rates due to their multi-functional groups (hydroxy, hydroperoxy, and C-C double bond) [18-19, 67]. Several of these reactions likely lead to the formation of HOMs. In Scheme 5, we show an example route to the formation of a $C_{10}H_{16}O_{10}$ compound, one or more species having the same chemical formula have previously been detected by a NO_3^- CIMS and reaches daily maximum in the afternoon in the southeastern U.S. [68]. Peroxy radical R4 can undergo a rapid OOH-OO 1,7 H-shift to produce peroxy radical R11. The rate coefficient of similar H-shifts has been calculated to be on the order of 10^5 s^{-1} in other systems[67]. R11 can abstract the allylic H on C3 adjacent to the hydroxy group, the rate coefficient of which is calculated to be 0.37 s^{-1} for a RO_2 with similar structure (α-pinene *anti* 3-OH,8-RO_2). Then, following O_2 addition to C7, fast OOH-OO shift, shift of allylic H at C4, and O_2 addition to C4, a peroxy radical R16 is produced. R16 can undergo 1,5 H-shift by abstracting the enolic H which has been calculated in other systems to be extremely fast (~10^6 s^{-1} [69]) and produce alkyl radical R17. R17 reacts with O_2, undergoes a series of fast OOH-OO shifts, abstracts the H at C4 adjacent to –OOH (~ 0.1 s^{-1} in another system[70]), and finally eliminates a –OH to produce $C_{10}H_{16}O_{10}$. This is just one of many plausible routes (Scheme S4 and S5) leading to the formation of HOMs. RO_2 with chemical composition HO-$C_{10}H_{15}(OO)(OOH)O_2$, for example, have been detected in the OH

oxidation of α-pinene and β-pinene [21], suggestive of fast regenerative unimolecular reactions of RO_2 followed by O_2 addition, that is, RO_2 autoxidation.

Yields of Hydroxy Nitrates. Formation of HNs is an important process in atmospheric photochemistry. This pathway sequesters NO_x and thus inhibits oxidant formation [71]. In this study, we measure the overall yield of first generation α-pinene and β-pinene HNs ($C_{10}H_{17}NO_4$) to be 3.3±1.5% and 6.4±2.1%, respectively, at short $\tau_{bimolecular}$ ([NO]>1000 ppbv). The details regarding the instrumental sensitivity, the effect of secondary loss and gas/particle partitioning on the measured yields are discussed in SI section S5. The measured yields are much lower than those estimated from structure-activity-relationship (~30%) [72]. The monoterpene RO_2, however, have more complicated structures than most of the alkenes studied previously [63, 73-74]. Our values are consistent with a finding of Teng et al. [63] that internal alkenes have a lower yield of hydroxy nitrates than terminal alkenes with the same carbon number. Although poorly constrained in the literature, perhaps the nitrate yield from cyclic β-hydroxy RO_2 + NO is also lower than their non-cyclic counterparts. We estimate the nitrate branching ratio (BR_{RONO2}) of different RO_2 isomers and detailed discussions are included in the SI section S6 and Table S21.

The ring-opening fraction of alkyl radicals. As we find that only the ring-opened RO_2 undergo unimolecular reactions at appreciable rates, the importance of RO_2 unimolecular chemistry depends critically on the yield of the ring-opened RO_2 ($Y_{ring\text{-}opened\ RO2}$). $Y_{ring\text{-}opened\ RO2}$ can be calculated by Eqn. (3)

$$Y_{ring\text{-}opened\ RO2} = BR_{OH\_add} \times BR_{OH\_less\_sub} \times BR_{ring\text{-}open} \quad \text{Eqn. (3)}$$

where BR_{OH_add} represents the branching ratio of the OH chemistry proceeding via addition, $BR_{OH\_less\_sub}$ represents the branching ratio of OH adding onto the less-substituted olefinic carbon, and $BR_{ring\text{-}open}$ represents the branching ratio of the tertiary alkyl radical that opens the four-

membered ring. BR here is defined as the ratio of the rate constant for a particular product of a reaction to the rate constant for the total set of possible products[75].

Early theoretical studies estimate that BR_{OH_add} is 90% based on structure-activity relationships [4, 61]. The approximately 10% of the OH chemistry that proceeds via H-abstraction does not lead to ring opening.

For the OH addition, only the addition at the less-substituted olefinic carbon (i.e., C3 in α-pinene and C1 in β-pinene) leads to formation of tertiary alkyl radicals that can undergo ring opening (i.e., 3-OH,2-R• for α-pinene and 1-OH,2-R• for β-pinene). Previous studies calculated $BR_{OH\_less\_sub}$ as 50% and 93% for α-pinene and β-pinene, respectively[5, 61]. However, $BR_{OH\_less\_sub}$ is uncertain and not experimentally constrained yet. For example, the OH addition branching ratio of 2-methyl 2-butene, which shares some similarity to the substitutions on α-pinene C-C double bond, is 69% : 31% [63]. The uncertainties in the OH addition branching ratio will be propagated into the calculated $Y_{ring\text{-}opened\ RO2}$.

Regarding the opening of the four-membered ring, theoretical calculations show that this process is driven by the excess energy from OH addition; at room temperature, the canonical MC-TST rate coefficients for this process are much too slow to compete with the O_2-addition (Table S15 and Vereecken et al. [4]). Using RRKM theory at the CCSD(T)-F12a/VDZ-F12//ωB97X-D/aug-cc-pVTZ level), we calculate that at atmospheric pressure and room temperature $BR_{ring\text{-}open}$ is 32% and 44% for α-pinene 3-OH,2-R• and β-pinene 1-OH,2-R•, respectively (calculation details in SI Section S3). These $BR_{ring\text{-}open}$ are somewhat lower than those calculated by Vereecken et al. (50% and 70% for α-pinene and β-pinene, respectively)[4-5]. The calculated fractions are, however, highly sensitive to the energy barrier to break the four-membered ring and the assumed energy transfer per collision with bath gas (Tables S17 and S18). For example, as a sensitivity test we varied the

energy barrier to break the four-membered ring by ±1 kcal/mol (the estimated uncertainty in the calculated reaction barrier). This changes the calculated ring-opening fraction by about a factor of 2 in either direction for both monoterpenes. Table 1 briefly summarizes the above discussed branching ratios.

From the measured distribution of HNs under high NO condition, it is not possible to directly calculate $Y_{\text{ring-opened RO2}}$ because we do not know the nitrate branching ratio (BR_{RONO2}) for all RO_2. We suggest, however, that the ratio of the yield of α-pinene ring-opened RO_2 to that of β-pinene (i.e., $\frac{Yield_{\alpha-pinene\ 3-OH,8-OO}}{Yield_{\beta-pinene\ 1-OH,8-OO}}$) can be estimated from our HN measurements. As the ring-opened RO_2 of both terpenes share very similar structure (i.e., tertiary RO_2 in the $-C(CH_3)_2OO$ group), it is reasonable to assume that these RO_2 have similar BR_{RONO2}. Following this assumption, $\frac{Yield_{\alpha-pinene\ 3-OH,8-OO}}{Yield_{\beta-pinene\ 1-OH,8-OO}}$ should be similar to $\frac{Yield_{\alpha-pinene\ 3-OH,8-ONO_2}}{Yield_{\beta-pinene\ 1-OH,8-ONO_2}}$. At [NO] > 1000ppb, $\frac{Yield_{\alpha-pinene\ 3-OH,8-ONO_2}}{Yield_{\beta-pinene\ 1-OH,8-ONO_2}}$ is 2.7 (i.e., $\frac{1.6\%}{0.6\%}$). Thus, we suggest $\frac{Yield_{\alpha-pinene\ 3-OH,8-OO}}{Yield_{\beta-pinene\ 1-OH,8-OO}}$ to be 2.7 - much large than theoretical calculation by using Eqn. (3) (i.e., 0.39 as shown Table 1).

To go further, we infer the $BR_{\text{ring-open}}$ of both terpenes by making additional assumptions about BR_{RONO2} and solving system of equations. If we assume that all the β-hydroxy RO_2 have the same BR_{RONO2} (denoted as $BR_{RONO2,\beta\text{-OH}}$) according to Teng et al.[16] and assume that the ring-opened RO_2 of both α-pinene and β-pinene have the same BR_{RONO2} (denoted as $BR_{RONO2,\text{ring-open}}$), we can express the measured yields of six hydroxy nitrate isomers (α-pinene and β-pinene combined) as the product of branching ratio of each step as shown below,

$$Y_{\alpha\text{-pinene 3-OH,8-ONO2}} = BR_{OH\_add} \times BR_{add\_C3} \times BR_{\alpha\text{-pinene,ring-open}} \times BR_{RONO2,\text{ring-open}}$$

$$Y_{\alpha\text{-pinene 3-OH,2-ONO2}} = BR_{OH\_add} \times BR_{add\_C3} \times (1- BR_{\alpha\text{-pinene,ring-open}}) \times BR_{RONO2,\beta\text{-OH}}$$

$$Y_{\alpha\text{-pinene 2-OH,3-ONO2}} = BR_{OH\_add} \times (1\text{-}BR_{add\_C3}) \times BR_{RONO2,\beta\text{-OH}}$$

$$Y_{\beta\text{-pinene 1-OH,8-ONO2}} = BR_{OH\_add} \times BR_{add\_C1} \times BR_{\beta\text{-pinene,ring-open}} \times BR_{RONO2,ring\text{-}open}$$

$$Y_{\beta\text{-pinene 1-OH,2-ONO2}} = BR_{OH\_add} \times BR_{add\_C1} \times (1\text{-}BR_{\beta\text{-pinene,ring-open}}) \times BR_{RONO2,\beta\text{-OH}}$$

$$Y_{\beta\text{-pinene 2-OH,1-ONO2}} = BR_{OH\_add} \times (1\text{-}BR_{add\_C1}) \times BR_{RONO2,\beta\text{-OH}}$$

where BR_{add_C3} and BR_{add_C1} represent the branching ratio of OH adding onto C3 and C1 in α-pinene and β-pinene, respectively. BR_{OH_add} is 0.9 as discussed above. BR_{add_C3}, BR_{add_C1}, $BR_{\alpha\text{-pinene,ring-open}}$, $BR_{\beta\text{-pinene,ring-open}}$, $BR_{RONO2,\beta\text{-OH}}$, and $BR_{RONO2,ring\text{-}open}$ are unknowns. By solving the system of equations (six unknowns and six equations), we find that $BR_{ring\text{-}open}$ is 97% and 34% for α-pinene and β-pinene, respectively.

Similarly, if we assume that the ratio of BR_{RONO2} for tertiary, secondary, and primary β-hydroxy RO_2 is 1.25: 1: 0.75 as suggested by Wennberg et al.[72], $BR_{ring\text{-}open}$ is found to be 97% and 36% for α-pinene and β-pinene, respectively (SI section S6). The discussions on the other inferred parameters, such as BR_{RONO2}, can be found in the SI section S6. In summary, this analysis suggests that essentially all the tertiary alkyl radicals formed in OH + α-pinene (i.e., 3-OH,2-R•) ring-open while only ~1/3 of those do so for β-pinene. As the BR_{RONO2} exhibits highly complicated dependence on molecular size, structure, and functionality, we place very low confidence in these estimates. However, we place much higher confidence in the ratio of the yield of α-pinene ring-opened RO_2 to that of β-pinene (i.e., 2.7).

One approach used in the literature to evaluate the ring-opening fraction has been to compare the measured yields of oxidation products, such as pinonaldehyde and acetone, with the theoretical yield obtained by propagating the branching ratio of each step (e.g., Scheme S7)[4]. For example, using a ring-opening fraction of 50% and branching ratios of other reaction steps (SI

section S6), Peeters et al. calculated the pinonaldehyde yield from α-pinene photooxidation to be 59.5%[61]. This yield is about twice as the measured yield (27-35%)[2, 76-77] under conditions similar to theoretical calculation (see SI section S6 for more discussions). Using the highly uncertain branching ratios inferred above based on Wennberg et al.[72] suggested BR_{RONO2}, the implied pinonaldehyde yield is 17% (2% from 3-OH,2-RO_2 and 15% from 2-OH,3-RO_2).

In addition to pinonaldehyde, acetone yields have also been used to estimate the ring-opening fraction. Acetone has been proposed to be the major decomposition product of ring-opened hydroxy alkoxy radicals (see Scheme 4 for α-pinene). However, an earlier theoretical study suggested that the endo-cyclization of R1 has an extremely low barrier, which is about 3.6 kcal mol^{-1} lower than that of acetone elimination[60] – consistent with the formation of the $C_{10}H_{17}NO_5$ hydroxy nitrates described above. Thus, the endo-cyclization easily outruns the acetone elimination reaction. An alternative formation pathway for acetone has been proposed in Vereecken et al.[60] Experimental evidence from this study supports this theoretically-based prediction: we observe a very low yield of $C_7H_{11}NO_4$, 0.2% (assuming the same sensitivity as $C_{10}H_{17}NO_4$), which is expected as a co-product of acetone elimination (Scheme S7). This yield is ten times smaller than expected based on the measured acetone yield (10%)[77] and an assumed 20% nitrate branching ratio (using cyclohexane as a surrogate)[78]. Thus, acetone elimination is likely only a minor pathway of the ring-opened alkoxy radical and thus not a good constraint on the ring-opening fraction.

Conclusions

Unimolecular reactions of ring-opened RO_2 in the OH oxidation of α-pinene (4±2 s^{-1}) and β-pinene (16±5 s^{-1}) are shown here to outrun bimolecular chemistry in the atmosphere. While the ring-opening fraction of alkyl radical remains highly uncertain, our results suggest that this fraction is

roughly a factor of three larger for α-pinene than β-pinene. This ring-opening fraction determines the yield of ring-opened RO_2 formed in both α-pinene and β-pinene systems and the extent to which the RO_2 unimolecular reactions occur.

In contrast to RO_2 bimolecular reactions with NO, the unimolecular reactions do not convert NO to NO_2 and hence influence the O_3 formation. This unimolecular chemistry, currently not considered in atmospheric models, may lead to an over-prediction in O_3 formation rate by models[79]. On the other hand, the low rate of nitrate formation compared with estimates using structure-activity relationships, may reduce the simulated loss of NO_x due to organic nitrates, impacting ozone formation in the opposite direction. In addition, as shown in many reaction schemes in this study, hydroxyl radical or hydroperoxyl radical are likely generated at the termination step of unimolecular reactions. A detailed understanding on the sensitivity of atmospheric oxidation capacity to unimolecular reactions such as these warrants further modeling studies.

The unknown kinetics of RO_2 unimolecular reactions has been a prominent challenge to unravel the exact formation mechanisms of HOMs. The fast unimolecular reactions of α-pinene and β-pinene ring-opened RO_2 described here support the hypothesis that formation of HOMs via autoxidation occurs for monoterpenes on relevant timescales. These HOMs are important contributors to ambient monoterpene organic aerosol (OA), suggested as the largest source of summertime OA in the southeastern U.S.[7, 12].

Finally, the *ab initio* calculations, together with the detection of unimolecular reaction products, imply that the unimolecular reactions of ring-opened RO_2 are enhanced by the presence of C-C double bond and the hydroxy group. In light of this, it is likely that RO_2 from other

monoterpene species, such as limonene, terpinolene, and myrcene, also undergo similar fast unimolecular reactions and deserve further study.

ASSOCIATED CONTENT

Supporting Information

Additional information on the peak identification of α-pinene and β-pinene hydroxy nitrates, mathematical derivations to show the relationship between the (ring-opened HN):(ring-retained HNs) ratio and RO_2 bimolecular and unimolecular lifetimes, calculation of $\tau_{bimolecular}$, computational approach, kinetic box model to calculate the rate of unimolecular reactions, discussions of yields of α-pinene and β-pinene hydroxy nitrates, discussions of uncertainties associated with the branching ratios, and discussions of nitrate branching ratio.

Output files of all calculations including the xyz-geometries can be found online at: https://sid.erda.dk/sharelink/hYtUUanavY

ACKNOWLEDGMENTS

We thank Eric Praske, Krystal T. Vasquez, and Yuanlong Huang for technical support. LX, JDC, and POW acknowledge NASA (NNX14AP46G) and NSF (CHE-1508526) for supporting this work. KHM, RVO, and HGK acknowledge funding from the University of Copenhagen. KHM acknowledges the financial support of the Danish Ministry for Higher Education and Science's Elite Research travel grant

AUTHOR INFORMATION

Corresponding Authors

* E-mail: luxu@caltech.edu

* E-mail: wennberg@caltech.edu

* E-mail: hgk@chem.ku.dk

ORCID

Lu Xu: 0000-0002-0021-9876

Kristian H. Møller: 0000-0001-8070-8516

John D. Crounse: 0000-0001-5443-729X

Rasmus V. Otkjær: 0000-0002-6094-1828

Henrik G. Kjaergaard: 0000-0002-7275-8297

Paul O. Wennberg: 0000-0002-6126-3854

Notes: the authors declare no competing financial interest.

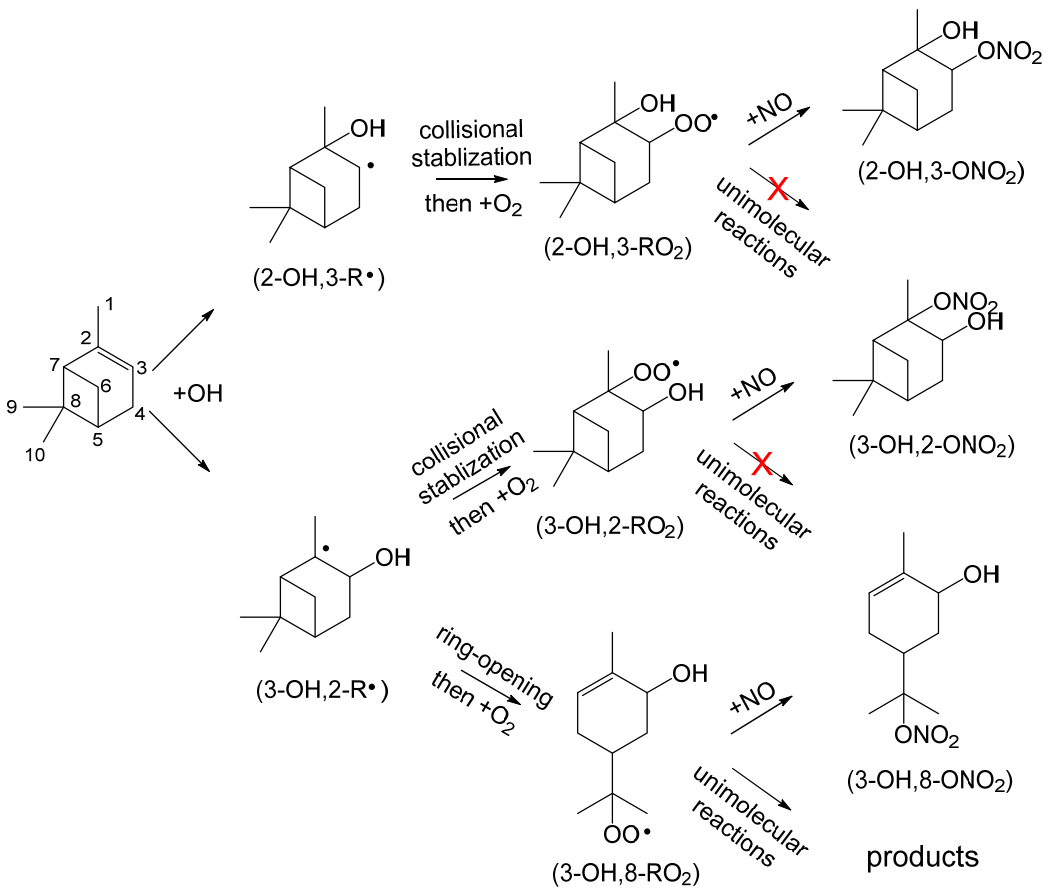

512

513 Scheme 1. The simplified oxidation mechanism of α-pinene. Each structural isomer of RO_2 and
514 hydroxy nitrate has multiple stereoisomers, which are shown in Scheme S2. The $RO+NO_2$
515 produced from RO_2+NO are not included in the scheme to improve clarity.

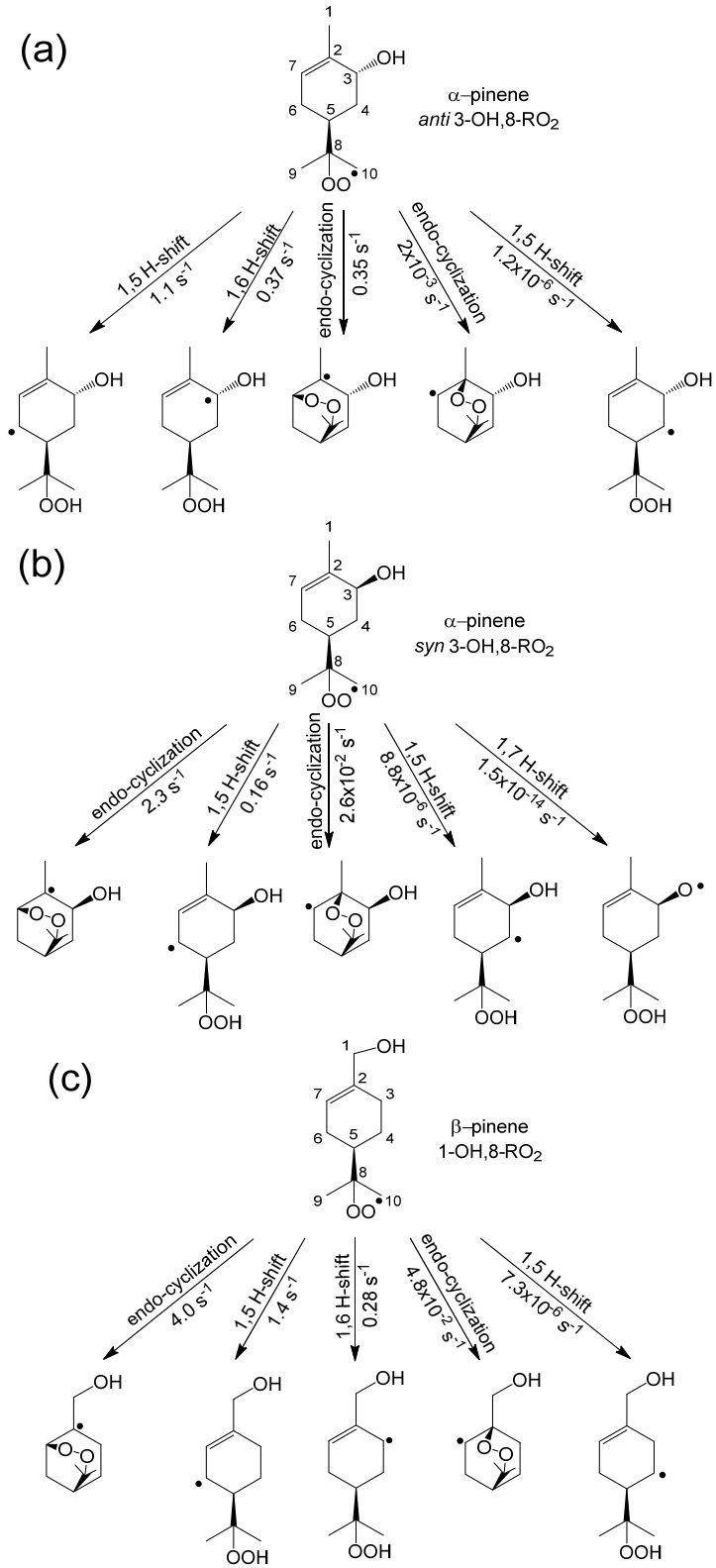

Scheme 2. Unimolecular reaction channels for (a) α-pinene *anti* 3-OH,8-RO_2; (b) α-pinene *syn* 3-OH,8-RO_2 and (c) β-pinene 1-OH,8-RO_2. Rate coefficients are calculated with the MC-TST approach by Møller et al. [23] at 298.15 K.

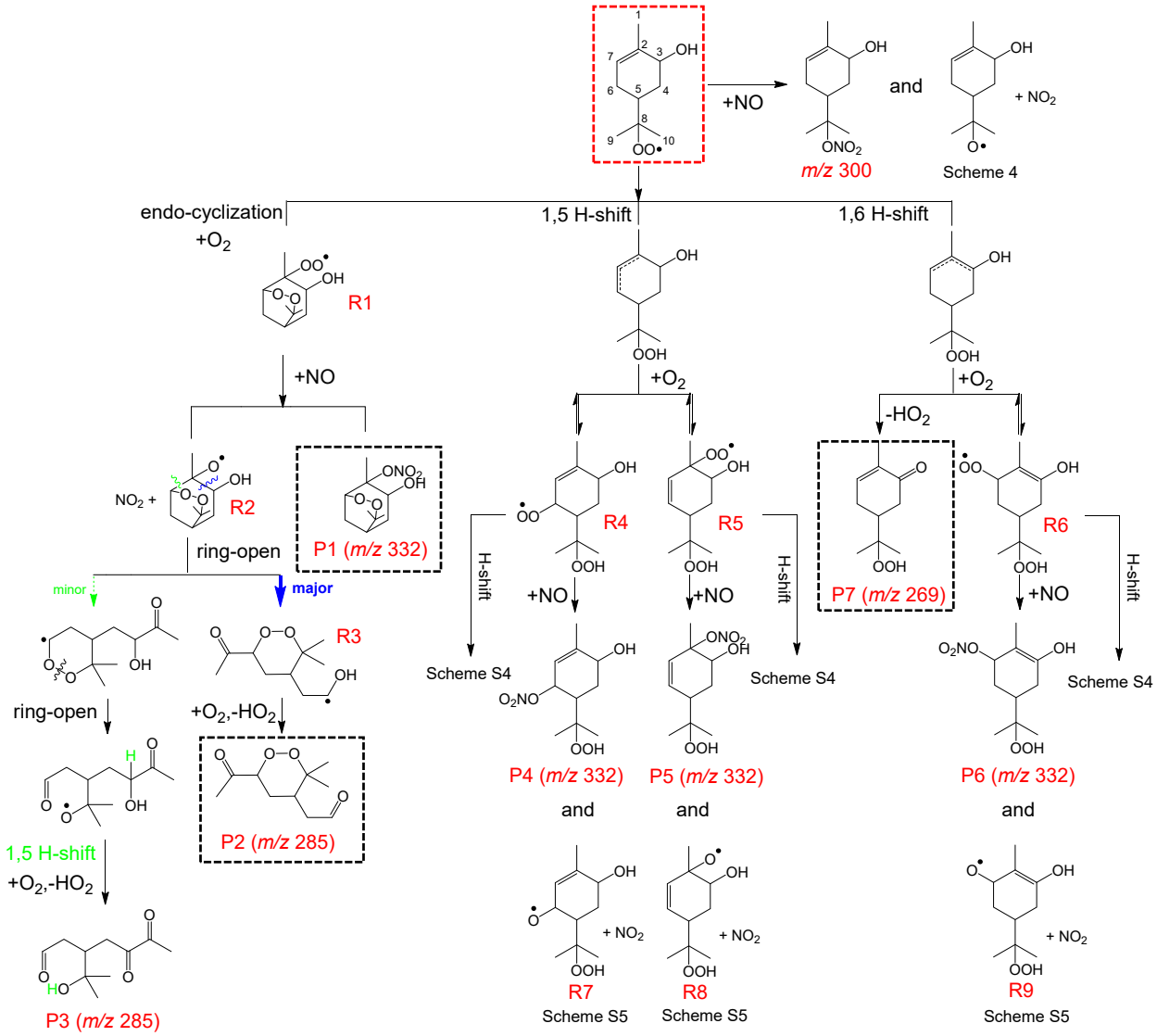

Scheme 3. The unimolecular reaction products of α-pinene 3-OH,8-RO_2 (shown in red box). The stereoisomers are not distinguished in this scheme. The 1,6 H-shift only occurs for *anti* 3-OH,8-RO_2. Observed species are shown in black boxes. The *m/z* listed below observed species are for the complex with CF_3O^- (molecular mass + 85).

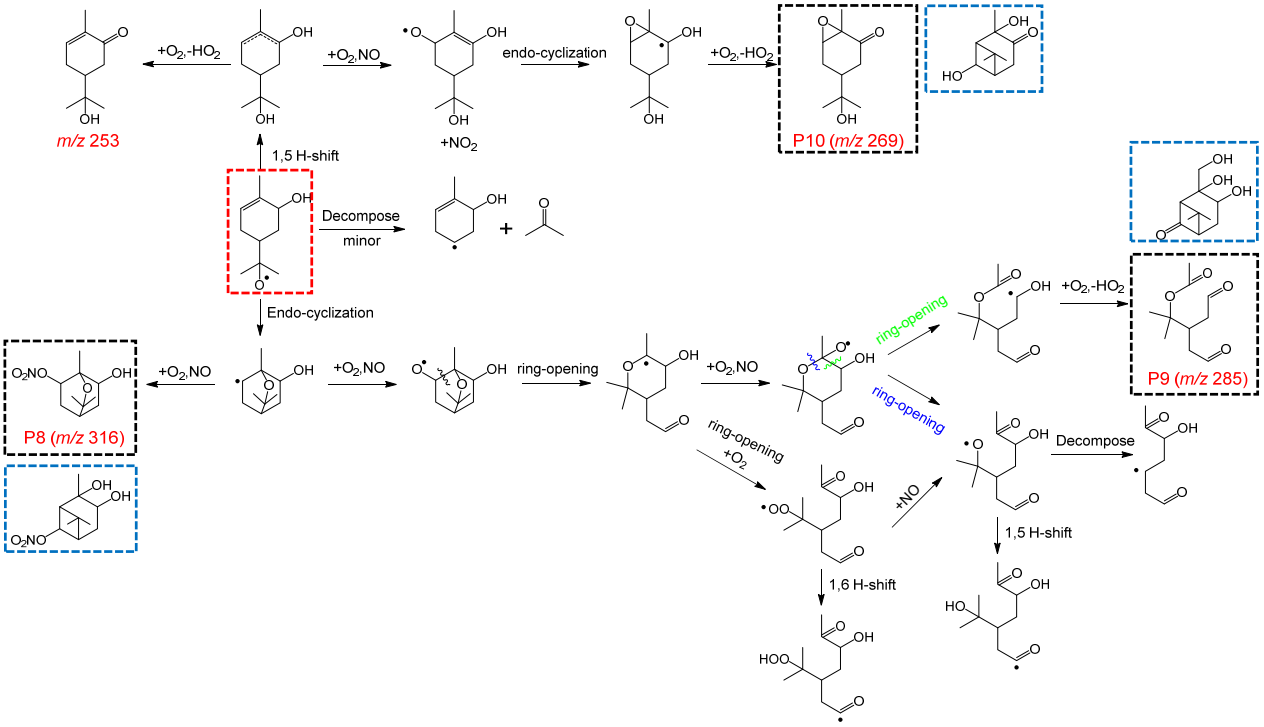

528

529 Scheme 4. Speculations on the reactions of α-pinene 3-OH,8-RO alkoxy radical (shown in red box)
530 at short $\tau_{bimolecular}$. The *m/z* listed below observed species are for the complex with CF_3O^-
531 (molecular mass + 85). Species having molecular weight consistent with observed signals are
532 shown in black box. The products proposed by Aschmann et al. [66] are shown in blue boxes. NO_2
533 produced from RO_2+NO is not shown in the figure.

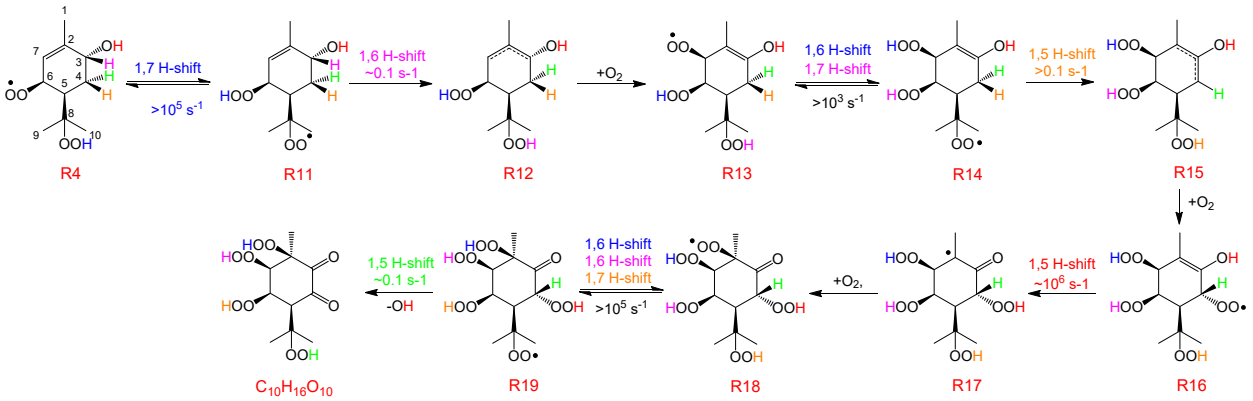

534

535 Scheme 5. An example pathway from α-pinene ring-opened RO_2 leading to the production of
536 highly oxygenated molecules. Unimolecular rate coefficients estimated from similar H-shifts at
537 298.15 K.

538

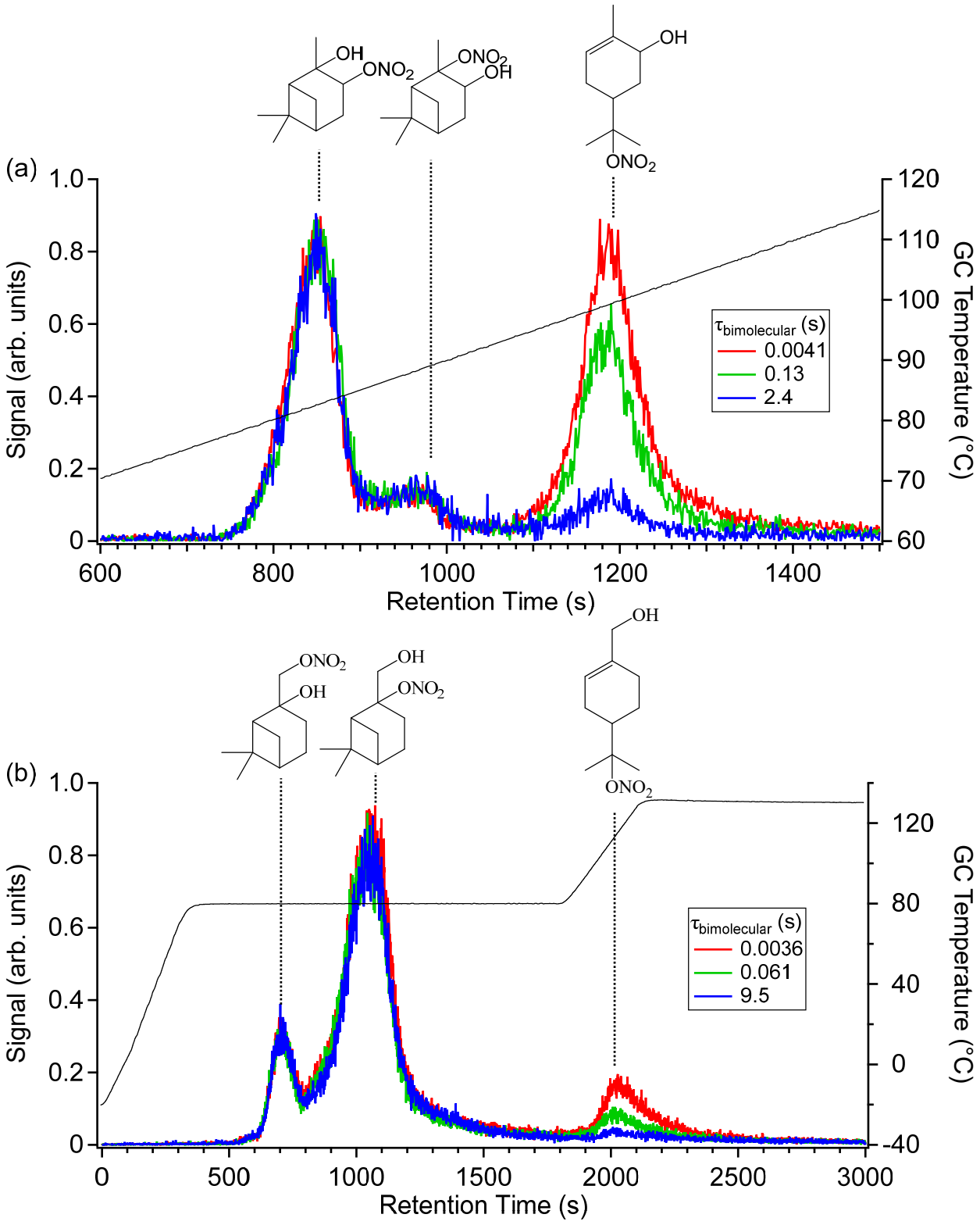

Figure 1. Chromatograms of hydroxy nitrates of (a) α-pinene and (b) β-pinene. The structural assignment of GC peaks is discussed in the SI section S1. In each panel, the GC chromatograms for three different RO_2 bimolecular lifetimes ($\tau_{bimolecular}$) are shown. The signals are scaled to match the magnitude of the ring-retained hydroxy nitrates. The black solid line shows the GC temperature.

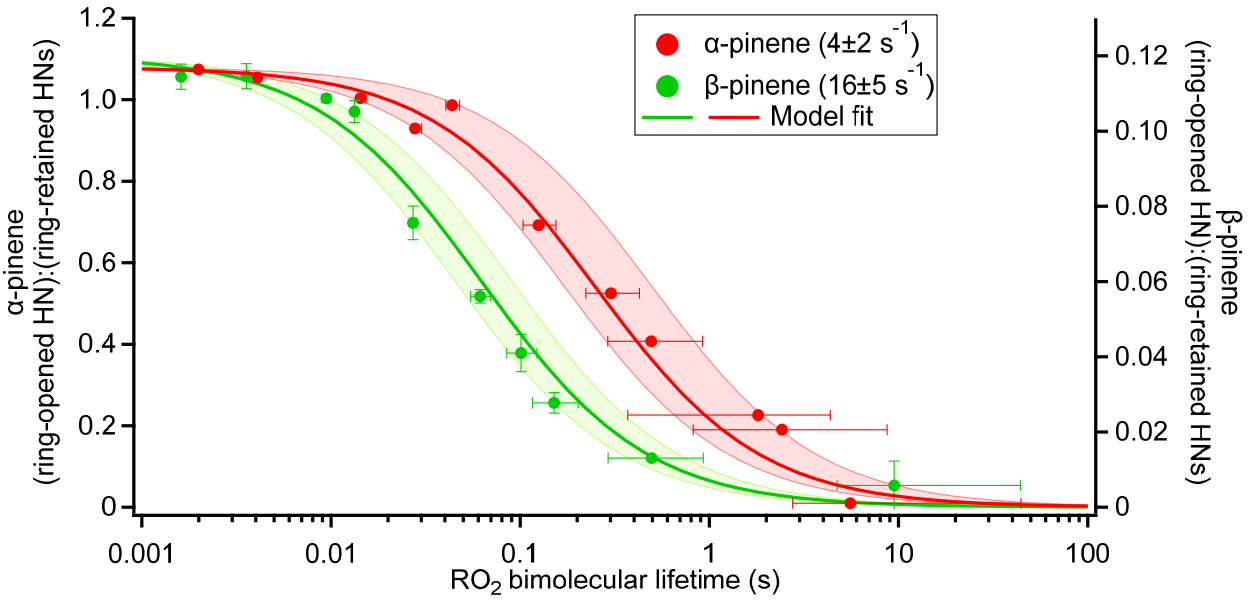

Figure 2. Ratio of ring-opened HN to ring-retained HNs of α-pinene and β-pinene as a function of RO_2 bimolecular lifetime. The uncertainty in RO_2 bimolecular lifetime is represented by the range from the beginning to the end of the photooxidation period. The solid line represents the experimentally determined average rate coefficient of unimolecular reactions of the ring-opened RO_2s. The shaded regions represent the range of uncertainty in the rate coefficients of unimolecular reactions.

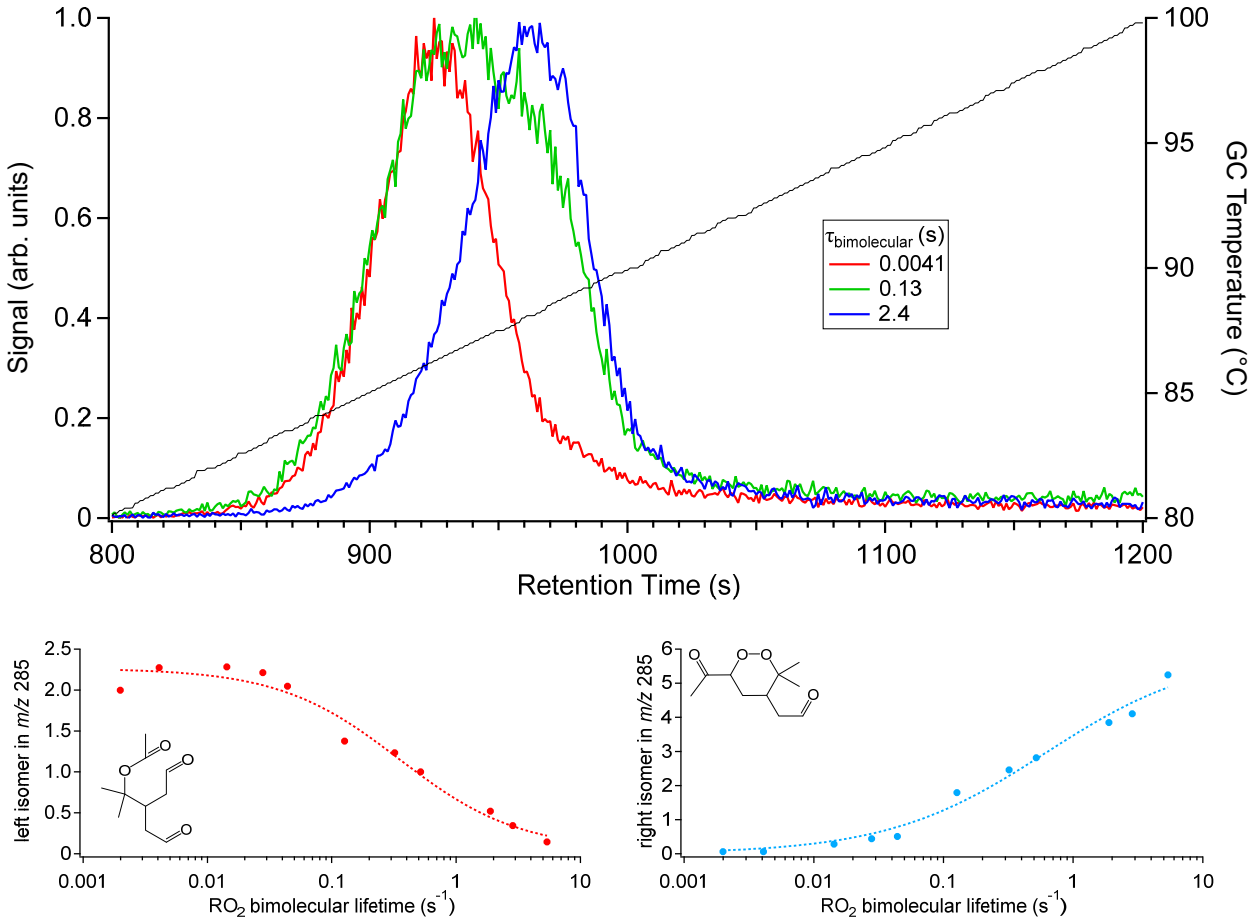

Figure 3. (Top) GC chromatograms of *m/z* 285 in α-pinene photooxidation experiments under different $\tau_{bimolecular}$. The signal is scaled by that of ring-retained HNs. H/D exchange analysis reveals that neither compound have acidic H. The proposed structures and the abundances of both peaks as a function of $\tau_{bimolecular}$ are shown in the bottom two panels.

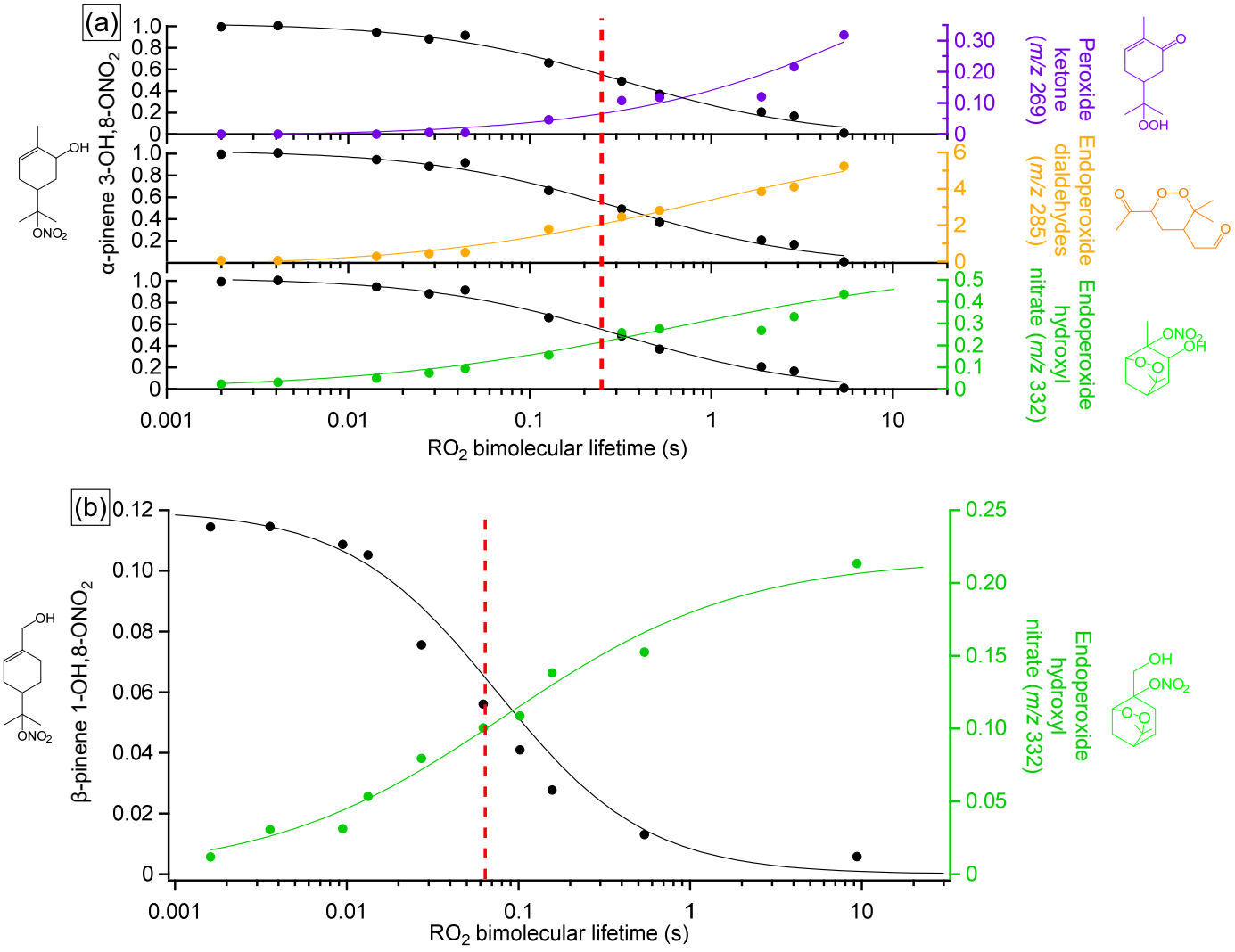

Figure 4. End products from unimolecular reactions of (a) α-pinene and (b) β-pinene as a function of RO_2 bimolecular lifetime. Data are normalized by the abundance of ring-retained hydroxy nitrates. The red dashed line indicates the unimolecular lifetime of ring-opened RO_2 at 296 K.

Table 1. The theoretically calculated yields of ring-opened RO_2 and the branching ratios along its formation pathway of both α-pinene and β-pinene.

Compound	Reference	BR_{OH_add}[a]	$BR_{OH\_less\text{-}sub}$[b]	$BR_{ring\text{-}open}$[c]	$Yield_{ring\text{-}opened\ RO2}$[d,e]
α-pinene	Vereecken et al. (2000)[4]	0.9	0.5	0.5	0.23
	This work	-	-	0.32[f]	-
β-pinene	Vereecken et al. (2012)[5]	0.9	0.93	0.7	0.59
	This work	-	-	0.44	-

[a]BR_{OH_add} represents the branching ratio that terpene+OH proceeds via addition to the double bond.

[b]$BR_{OH\_less\_sub}$ represents the branching ratio that OH adds to the less-substituted olefinic carbon (i.e., C3 and C1 in α-pinene and β-pinene, respectively).

[c]$BR_{ring\text{-}open}$ represents the ring-opening fraction of the activated tertiary alkyl radical.

[d]$Yield_{ring\text{-}opened\ RO2}$ represents that the yield of ring-opened RO_2. $Yield_{ring\text{-}opened\ RO2} = BR_{OH\_add} \times BR_{OH\_less\text{-}sub} \times BR_{ring\text{-}open}$.

[e]The ratio of α-pinene $Yield_{ring\text{-}opened\ RO2}$ relative to that of β-pinene is 0.39 based on studies of Vereecken et al. However, a ratio of 2.7 is derived from our measured yield of ring-opened hydroxy nitrate and an assumption that the nitrate branching ratio of ring-opened RO_2 is the same for both terpenes.

[f]α-pinene ring-opened RO_2 has two isomers, *syn* and *anti*. The calculated $BR_{ring\text{-}open}$ only differs by 0.02 between the two isomers (shown in Table S15). Here we report the average value. The calculated values are highly sensitive to the energy barrier to break the four-membered ring and the energy transfer per collision with bath gas (Tables S17 and S18).

References

1. Guenther, A.; Jiang, X.; Heald, C. L.; Sakulyanontvittaya, T.; Duhl, T.; Emmons, L. K.; Wang, X. The Model of Emissions of Gases and Aerosols from Nature Version 2.1 (Megan2.1): An Extended and Updated Framework for Modeling Biogenic Emissions. *Geosci. Model Dev.* **2012,** *5*, 1471-1492.
2. Eddingsaas, N. C.; Loza, C. L.; Yee, L. D.; Seinfeld, J. H.; Wennberg, P. O. A-Pinene Photooxidation under Controlled Chemical Conditions – Part 1: Gas-Phase Composition in Low- and High-Nox Environments. *Atmos. Chem. Phys.* **2012,** *12*, 6489-6504.
3. Lee, A.; Goldstein, A. H.; Keywood, M. D.; Gao, S.; Varutbangkul, V.; Bahreini, R.; Ng, N. L.; Flagan, R. C.; Seinfeld, J. H. Gas-Phase Products and Secondary Aerosol Yields from the Ozonolysis of Ten Different Terpenes. *J. Geophys. Res. - Atmos* **2006,** *111*.
4. Vereecken, L.; Peeters, J. Theoretical Study of the Formation of Acetone in the Oh-Initiated Atmospheric Oxidation of A-Pinene. *J. Phys. Chem. A* **2000,** *104*, 11140-11146.
5. Vereecken, L.; Peeters, J. A Theoretical Study of the Oh-Initiated Gas-Phase Oxidation Mechanism of B-Pinene (C10h16): First Generation Products. *Phys. Chem. Chem. Phys.* **2012,** *14*, 3802-3815.
6. Yu, J.; Cocker, D. R.; Griffin, R. J.; Flagan, R. C.; Seinfeld, J. H. Gas-Phase Ozone Oxidation of Monoterpenes: Gaseous and Particulate Products. *J. Atmos. Chem.* **1999,** *34*, 207-258.
7. Zhang, H.; Yee, L. D.; Lee, B. H.; Curtis, M. P.; Worton, D. R.; Isaacman-VanWertz, G.; Offenberg, J. H.; Lewandowski, M.; Kleindienst, T. E.; Beaver, M. R., et al. Monoterpenes Are the Largest Source of Summertime Organic Aerosol in the Southeastern United States. *Proc. Natl. Acad. Sci. U. S. A* **2018,** *115*, 2038-2043.
8. Ng, N. L.; Brown, S. S.; Archibald, A. T.; Atlas, E.; Cohen, R. C.; Crowley, J. N.; Day, D. A.; Donahue, N. M.; Fry, J. L.; Fuchs, H., et al. Nitrate Radicals and Biogenic Volatile Organic Compounds: Oxidation, Mechanisms, and Organic Aerosol. *Atmos. Chem. Phys.* **2017,** *17*, 2103-2162.
9. Ehn, M.; Thornton, J. A.; Kleist, E.; Sipila, M.; Junninen, H.; Pullinen, I.; Springer, M.; Rubach, F.; Tillmann, R.; Lee, B., et al. A Large Source of Low-Volatility Secondary Organic Aerosol. *Nature* **2014,** *506*, 476-479.
10. Pye, H. O. T.; Chan, A. W. H.; Barkley, M. P.; Seinfeld, J. H. Global Modeling of Organic Aerosol: The Importance of Reactive Nitrogen (Nox and No3). *Atmos. Chem. Phys.* **2010,** *10*, 11261-11276.
11. Kanakidou, M.; Seinfeld, J. H.; Pandis, S. N.; Barnes, I.; Dentener, F. J.; Facchini, M. C.; Van Dingenen, R.; Ervens, B.; Nenes, A.; Nielsen, C. J., et al. Organic Aerosol and Global Climate Modelling: A Review. *Atmos. Chem. Phys.* **2005,** *5*, 1053-1123.
12. Xu, L.; Pye, H. O. T.; He, J.; Chen, Y.; Murphy, B. N.; Ng, N. L. Experimental and Model Estimates of the Contributions from Biogenic Monoterpenes and Sesquiterpenes to Secondary Organic Aerosol in the Southeastern United States. *Atmos. Chem. Phys.* **2018,** *18*, 12613-12637.
13. Isaacman-VanWertz, G.; Massoli, P.; O'Brien, R.; Lim, C.; Franklin, J. P.; Moss, J. A.; Hunter, J. F.; Nowak, J. B.; Canagaratna, M. R.; Misztal, P. K., et al. Chemical Evolution of Atmospheric Organic Carbon over Multiple Generations of Oxidation. *Nat. Chem.* **2018,** *10*, 462-468.

14. Kroll, J. H.; Seinfeld, J. H. Chemistry of Secondary Organic Aerosol: Formation and Evolution of Low-Volatility Organics in the Atmosphere. *Atmospheric Environ.* **2008,** *42*, 3593-3624.
15. Orlando, J. J.; Tyndall, G. S. Laboratory Studies of Organic Peroxy Radical Chemistry: An Overview with Emphasis on Recent Issues of Atmospheric Significance. *Chem. Soc. Rev.* **2012,** *41*, 6294-6317.
16. Teng, A. P.; Crounse, J. D.; Wennberg, P. O. Isoprene Peroxy Radical Dynamics. *J. Am. Chem. Soc.* **2017,** *139*, 5367-5377.
17. Peeters, J.; Nguyen, T. L.; Vereecken, L. Hox Radical Regeneration in the Oxidation of Isoprene. *Phys. Chem. Chem. Phys.* **2009,** *11*, 5935-5939.
18. Praske, E.; Otkjær, R. V.; Crounse, J. D.; Hethcox, J. C.; Stoltz, B. M.; Kjaergaard, H. G.; Wennberg, P. O. Atmospheric Autoxidation Is Increasingly Important in Urban and Suburban North America. *Proc. Natl. Acad. Sci. U. S. A* **2018,** *115*, 64-69.
19. Crounse, J. D.; Nielsen, L. B.; Jørgensen, S.; Kjaergaard, H. G.; Wennberg, P. O. Autoxidation of Organic Compounds in the Atmosphere. *J. Phys. Chem. Lett* **2013,** *4*, 3513-3520.
20. Vereecken, L.; Peeters, J. Nontraditional (Per)Oxy Ring-Closure Paths in the Atmospheric Oxidation of Isoprene and Monoterpenes. *J. Phys. Chem. A* **2004,** *108*, 5197-5204.
21. Berndt, T.; Richters, S.; Jokinen, T.; Hyttinen, N.; Kurtén, T.; Otkjær, R. V.; Kjaergaard, H. G.; Stratmann, F.; Herrmann, H.; Sipilä, M., et al. Hydroxyl Radical-Induced Formation of Highly Oxidized Organic Compounds. *Nat. Commun.* **2016,** *7*, 13677.
22. Zhao, Y.; Thornton, J. A.; Pye, H. O. T. Quantitative Constraints on Autoxidation and Dimer Formation from Direct Probing of Monoterpene-Derived Peroxy Radical Chemistry. *Proc. Natl. Acad. Sci. U. S. A* **2018,** *115*, 12142-12147.
23. Møller, K. H.; Otkjær, R. V.; Hyttinen, N.; Kurtén, T.; Kjaergaard, H. G. Cost-Effective Implementation of Multiconformer Transition State Theory for Peroxy Radical Hydrogen Shift Reactions. *J. Phys. Chem. A* **2016,** *120*, 10072-10087.
24. Vereecken, L.; Peeters, J. The 1,5-H-Shift in 1-Butoxy: A Case Study in the Rigorous Implementation of Transition State Theory for a Multirotamer System. *J. Chem. Phys.* **2003,** *119*, 5159-5170.
25. Sharpe, S. W.; Johnson, T. J.; Sams, R. L.; Chu, P. M.; Rhoderick, G. C.; Johnson, P. A. Gas-Phase Databases for Quantitative Infrared Spectroscopy. *Appl. Spectrosc.* **2004,** *58*, 1452-1461.
26. Taylor, W. D.; Allston, T. D.; Moscato, M. J.; Fazekas, G. B.; Kozlowski, R.; Takacs, G. A. Atmospheric Photo-Dissociation Lifetimes for Nitromethane, Methyl Nitrite, and Methyl Nitrate. *Int. J. Chem. Kinet.* **1980,** *12*, 231-240.
27. Vasquez, K. T.; Allen, H. M.; Crounse, J. D.; Praske, E.; Xu, L.; Noelscher, A. C.; Wennberg, P. O. Low-Pressure Gas Chromatography with Chemical Ionization Mass Spectrometry for Quantification of Multifunctional Organic Compounds in the Atmosphere. *Atmos. Meas. Tech.* **2018,** *11*, 6815-6832.
28. Jenkin, M. E.; Saunders, S. M.; Pilling, M. J. The Tropospheric Degradation of Volatile Organic Compounds: A Protocol for Mechanism Development. *Atmospheric Environ.* **1997,** *31*, 81-104.
29. Saunders, S. M.; Jenkin, M. E.; Derwent, R. G.; Pilling, M. J. Protocol for the Development of the Master Chemical Mechanism, Mcm V3 (Part a): Tropospheric Degradation of Non-Aromatic Volatile Organic Compounds. *Atmos. Chem. Phys.* **2003,** *3*, 161-180.

30. Crounse, J. D.; Paulot, F.; Kjaergaard, H. G.; Wennberg, P. O. Peroxy Radical Isomerization in the Oxidation of Isoprene. *Phys. Chem. Chem. Phys.* **2011,** *13*, 13607-13613.
31. Werner, H.-J.; Knizia, G.; Manby, F. R. Explicitly Correlated Coupled Cluster Methods with Pair-Specific Geminals. *Mol. Phys.* **2011,** *109*, 407-417.
32. Halgren, T. A. Mmff Vii. Characterization of Mmff94, Mmff94s, and Other Widely Available Force Fields for Conformational Energies and for Intermolecular-Interaction Energies and Geometries. *J. Comput. Chem.* **1999,** *20*, 730-748.
33. Halgren, T. A. Merck Molecular Force Field. V. Extension of Mmff94 Using Experimental Data, Additional Computational Data, and Empirical Rules. *J. Comput. Chem.* **1996,** *17*, 616-641.
34. Halgren, T. A.; Nachbar, R. B. Merck Molecular Force Field. Iv. Conformational Energies and Geometries for Mmff94. *J. Comput. Chem.* **1996,** *17*, 587-615.
35. Halgren, T. A. Merck Molecular Force Field. Iii. Molecular Geometries and Vibrational Frequencies for Mmff94. *J. Comput. Chem.* **1996,** *17*, 553-586.
36. Halgren, T. A. Merck Molecular Force Field. Ii. Mmff94 Van Der Waals and Electrostatic Parameters for Intermolecular Interactions. *J. Comput. Chem.* **1996,** *17*, 520-552.
37. Halgren, T. A. Merck Molecular Force Field. I. Basis, Form, Scope, Parameterization, and Performance of Mmff94. *J. Comput. Chem.* **1996,** *17*, 490-519.
38. *Spartan'16*, Wavefunction, Inc., Irvine, CA.
39. Frisch, M. J.; Trucks, G. W.; Schlegel, H. B.; Scuseria, G. E.; Robb, M. A.; Cheeseman, J. R.; Scalmani, G.; Barone, V.; Petersson, G. A.; Nakatsuji, H., et al. *Gaussian 16 Rev. A.03*, Wallingford, CT, 2016.
40. Becke, A. D. Density‐Functional Thermochemistry. Iii. The Role of Exact Exchange. *J. Chem. Phys.* **1993,** *98*, 5648-5652.
41. Lee, C.; Yang, W.; Parr, R. G. Development of the Colle-Salvetti Correlation-Energy Formula into a Functional of the Electron Density. *Phys. Rev. B* **1988,** *37*, 785-789.
42. Hehre, W. J.; Ditchfield, R.; Pople, J. A. Self—Consistent Molecular Orbital Methods. Xii. Further Extensions of Gaussian—Type Basis Sets for Use in Molecular Orbital Studies of Organic Molecules. *J. Chem. Phys.* **1972,** *56*, 2257-2261.
43. Clark, T.; Chandrasekhar, J.; Spitznagel, G. W.; Schleyer, P. V. R. Efficient Diffuse Function-Augmented Basis Sets for Anion Calculations. Iii. The 3-21+G Basis Set for First-Row Elements, Li–F. *J. Comput. Chem.* **1983,** *4*, 294-301.
44. Frisch, M. J.; Pople, J. A.; Binkley, J. S. Self‐Consistent Molecular Orbital Methods 25. Supplementary Functions for Gaussian Basis Sets. *J. Chem. Phys.* **1984,** *80*, 3265-3269.
45. Chai, J.-D.; Head-Gordon, M. Long-Range Corrected Hybrid Density Functionals with Damped Atom-Atom Dispersion Corrections. *Phys. Chem. Chem. Phys.* **2008,** *10*, 6615-6620.
46. Dunning Jr., T. H. Gaussian Basis Sets for Use in Correlated Molecular Calculations. I. The Atoms Boron through Neon and Hydrogen. *J. Chem. Phys.* **1989,** *90*, 1007-1023.
47. Kendall, R. A.; Dunning Jr., T. H.; Harrison, R. J. Electron Affinities of the First‐Row Atoms Revisited. Systematic Basis Sets and Wave Functions. *J. Chem. Phys.* **1992,** *96*, 6796-6806.
48. Adler, T. B.; Knizia, G.; Werner, H.-J. A Simple and Efficient Ccsd(T)-F12 Approximation. *Acc. Chem. Res.* **2007,** *127*, 221106.
49. Knizia, G.; Adler, T. B.; Werner, H.-J. Simplified Ccsd(T)-F12 Methods: Theory and Benchmarks. *J. Chem. Phys.* **2009,** *130*, 054104.
50. Peterson, K. A.; Adler, T. B.; Werner, H.-J. Systematically Convergent Basis Sets for Explicitly Correlated Wavefunctions: The Atoms H, He, B–Ne, and Al–Ar. *J. Chem. Phys.* **2008,** *128*, 084102.

51. Watts, J. D.; Gauss, J.; Bartlett, R. J. Coupled ‐ Cluster Methods with Noniterative Triple Excitations for Restricted Open ‐ Shell Hartree–Fock and Other General Single Determinant Reference Functions. Energies and Analytical Gradients. *J. Chem. Phys.* **1993,** *98*, 8718-8733.
52. Werner, H.-J.; Knizia, G.; R. Manby, F. Explicitly Correlated Coupled Cluster Methods with Pair-Specific Geminals. *Mol. Phys.* **2011,** *109*, 407-417.
53. Werner, H.-J.; Knowles, P. J.; Knizia, G.; Manby, F. R.; Schütz, M. Molpro: A General-Purpose Quantum Chemistry Program Package. *Wiley Interdiscip. Rev. Comput. Mol. Sci.* **2012,** *2*, 242-253.
54. Werner, H.-J.; Knowles, P. J.; Knizia, G.; Manby, F. R.; Schütz, M.; Celani, P.; Györffy, W.; Kats, D.; Korona, T.; Lindh, R., et al. *Molpro, Version 2012.1, a Package of Ab Initio Programs*, 2012.
55. Møller, K. H.; Bates, K. H.; Kjaergaard, H. G. The Importance of Peroxy Radical Hydrogen Shift Reactions in Atmospheric Isoprene Oxidation. *J. Phys. Chem. A* **2019**.
56. Matlab R2016b.
57. Eckart, C. The Penetration of a Potential Barrier by Electrons. *Phys. Rev.* **1930,** *35*, 1303-1309.
58. Glowacki, D. R.; Liang, C.-H.; Morley, C.; Pilling, M. J.; Robertson, S. H. Mesmer: An Open-Source Master Equation Solver for Multi-Energy Well Reactions. *J. Phys. Chem. A* **2012,** *116*, 9545-9560.
59. Otkjær, R. V.; Jakobsen, H. H.; Tram, C. M.; Kjaergaard, H. G. Calculated Hydrogen Shift Rate Constants in Substituted Alkyl Peroxy Radicals. *J. Phys. Chem. A* **2018,** *122*, 8665-8673.
60. Vereecken, L.; Muller, J. F.; Peeters, J. Low-Volatility Poly-Oxygenates in the Oh-Initiated Atmospheric Oxidation of A-Pinene: Impact of Non-Traditional Peroxyl Radical Chemistry. *Phys. Chem. Chem. Phys.* **2007,** *9*, 5241-5248.
61. Peeters, J.; Vereecken, L.; Fantechi, G. The Detailed Mechanism of the Oh-Initiated Atmospheric Oxidation of A-Pinene: A Theoretical Study. *Phys. Chem. Chem. Phys.* **2001,** *3*, 5489-5504.
62. Kurtén, T.; Møller, K. H.; Nguyen, T. B.; Schwantes, R. H.; Misztal, P. K.; Su, L.; Wennberg, P. O.; Fry, J. L.; Kjaergaard, H. G. Alkoxy Radical Bond Scissions Explain the Anomalously Low Secondary Organic Aerosol and Organonitrate Yields from A-Pinene + No3. *J. Phys. Chem. Lett* **2017**, 2826-2834.
63. Teng, A. P.; Crounse, J. D.; Lee, L.; St. Clair, J. M.; Cohen, R. C.; Wennberg, P. O. Hydroxy Nitrate Production in the Oh-Initiated Oxidation of Alkenes. *Atmos. Chem. Phys.* **2015,** *15*, 4297-4316.
64. Griffith, S. M.; Hansen, R. F.; Dusanter, S.; Michoud, V.; Gilman, J. B.; Kuster, W. C.; Veres, P. R.; Graus, M.; de Gouw, J. A.; Roberts, J., et al. Measurements of Hydroxyl and Hydroperoxy Radicals During Calnex-La: Model Comparisons and Radical Budgets. *J. Geophys. Res. - Atmos* **2016,** *121*, 4211-4232.
65. Hidy, G. M.; Blanchard, C. L.; Baumann, K.; Edgerton, E.; Tanenbaum, S.; Shaw, S.; Knipping, E.; Tombach, I.; Jansen, J.; Walters, J. Chemical Climatology of the Southeastern United States, 1999-2013. *Atmos. Chem. Phys.* **2014,** *14*, 11893-11914.
66. Aschmann, S. M.; Reissell, A.; Atkinson, R.; Arey, J. Products of the Gas Phase Reactions of the Oh Radical with A- and B-Pinene in the Presence of No. *J. Geophys. Res. - Atmos* **1998,** *103*, 25553-25561.

67. Jørgensen, S.; Knap, H. C.; Otkjær, R. V.; Jensen, A. M.; Kjeldsen, M. L. H.; Wennberg, P. O.; Kjaergaard, H. G. Rapid Hydrogen Shift Scrambling in Hydroperoxy-Substituted Organic Peroxy Radicals. *J. Phys. Chem. A* **2016,** *120*, 266-275.
68. Massoli, P.; Stark, H.; Canagaratna, M. R.; Krechmer, J. E.; Xu, L.; Ng, N. L.; Mauldin, R. L.; Yan, C.; Kimmel, J.; Misztal, P. K., et al. Ambient Measurements of Highly Oxidized Gas-Phase Molecules During the Southern Oxidant and Aerosol Study (Soas) 2013. *ACS Earth Space Chem.* **2018**.
69. Peeters, J.; Nguyen, T. L. Unusually Fast 1,6-H Shifts of Enolic Hydrogens in Peroxy Radicals: Formation of the First-Generation C2 and C3 Carbonyls in the Oxidation of Isoprene. *J. Phys. Chem. A* **2012,** *116*, 6134-6141.
70. Praske, E.; Otkjær, R. V.; Crounse, J. D.; Hethcox, J. C.; Stoltz, B. M.; Kjaergaard, H. G.; Wennberg, P. O. Intramolecular Hydrogen Shift Chemistry of Hydroperoxy-Substituted Peroxy Radicals. *J. Phys. Chem. A* **2019,** *123*, 590-600.
71. Paulot, F.; Henze, D. K.; Wennberg, P. O. Impact of the Isoprene Photochemical Cascade on Tropical Ozone. *Atmos. Chem. Phys.* **2012,** *12*, 1307-1325.
72. Wennberg, P. O.; Bates, K. H.; Crounse, J. D.; Dodson, L. G.; McVay, R. C.; Mertens, L. A.; Nguyen, T. B.; Praske, E.; Schwantes, R. H.; Smarte, M. D., et al. Gas-Phase Reactions of Isoprene and Its Major Oxidation Products. *Chem. Rev.* **2018,** *118*, 3337-3390.
73. Arey, J.; Aschmann, S. M.; Kwok, E. S. C.; Atkinson, R. Alkyl Nitrate, Hydroxyalkyl Nitrate, and Hydroxycarbonyl Formation from the Nox−Air Photooxidations of C5−C8 N-Alkanes. *J. Phys. Chem. A* **2001,** *105*, 1020-1027.
74. Matsunaga, A.; Ziemann, P. J. Yields of B-Hydroxynitrates, Dihydroxynitrates, and Trihydroxynitrates Formed from Oh Radical-Initiated Reactions of 2-Methyl-1-Alkenes. *Proc. Natl. Acad. Sci. U. S. A* **2010,** *107*, 6664-6669.
75. Cleaves, H. J., Branching Ratio. In *Encyclopedia of Astrobiology*, Gargaud, M.; Amils, R.; Quintanilla, J. C.; Cleaves, H. J.; Irvine, W. M.; Pinti, D. L.; Viso, M., Eds. Springer Berlin Heidelberg: Berlin, Heidelberg, 2011; pp 218-218.
76. Aschmann, S. M.; Atkinson, R.; Arey, J. Products of Reaction of Oh Radicals with A-Pinene. *J. Geophys. Res. - Atmos* **2002,** *107*, ACH 6-1-ACH 6-7.
77. Wisthaler, A.; Jensen, N. R.; Winterhalter, R.; Lindinger, W.; Hjorth, J. Measurements of Acetone and Other Gas Phase Product Yields from the Oh-Initiated Oxidation of Terpenes by Proton-Transfer-Reaction Mass Spectrometry (Ptr-Ms). *Atmospheric Environ.* **2001,** *35*, 6181-6191.
78. Espada, C.; Grossenbacher, J.; Ford, K.; Couch, T.; Shepson, P. B. The Production of Organic Nitrates from Various Anthropogenic Volatile Organic Compounds. *Int. J. Chem. Kinet.* **2005,** *37*, 675-685.
79. Travis, K. R.; Jacob, D. J.; Fisher, J. A.; Kim, P. S.; Marais, E. A.; Zhu, L.; Yu, K.; Miller, C. C.; Yantosca, R. M.; Sulprizio, M. P., et al. Why Do Models Overestimate Surface Ozone in the Southeast United States? *Atmos. Chem. Phys.* **2016,** *16*, 13561-13577.

TOC graphic

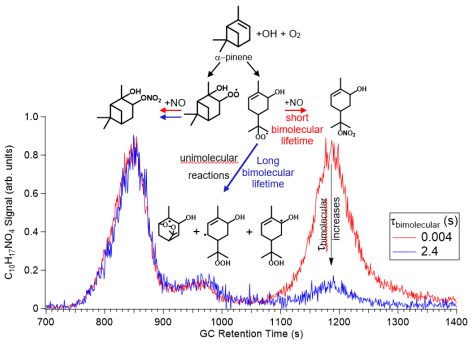
+OH + O2
α-pinene
+NO
+NO
short bimolecular lifetime
unimolecular reactions
Long bimolecular lifetime
τbimolecular increases
τbimolecular (s)
0.004
2.4
C10H17NO4 Signal (arb. units)
GC Retention Time (s)